AIP | The Journal of Chemical Physics

Merging and hopping processes in systems of ultrasoft, cluster forming particles under compression

Marta Montes-Saralegui, Arash Nikoubashman, and Gerhard Kahl

Citation: The Journal of Chemical Physics **141**, 124908 (2014); doi: 10.1063/1.4896055
View online: http://dx.doi.org/10.1063/1.4896055
View Table of Contents: http://scitation.aip.org/content/aip/journal/jcp/141/12?ver=pdfcov
Published by the AIP Publishing

Merging and hopping processes in systems of ultrasoft, cluster forming particles under compression

Marta Montes-Saralegui,[1,a)] Arash Nikoubashman,[2,b)] and Gerhard Kahl[1]
[1]*Institute of Theoretical Physics and CMS, Vienna University of Technology, Wiedner Hauptstraße 8-10, A-1040 Vienna, Austria*
[2]*Department of Chemical and Biological Engineering, Princeton University, Princeton, New Jersey 08544, USA*

(Received 8 July 2014; accepted 21 August 2014; published online 29 September 2014)

We have exposed a two-dimensional nanodrop of particles interacting via an ultrasoft (i.e., bounded), purely repulsive potential to a combined thermo- and barostat. While increasing the pressure steadily via a suitable pressure increment the temperature of the system is kept at a fixed target temperature. Once the hexagonal crystal composed of clusters of overlapping particles has formed, we investigate the system's reaction on the non-equilibrium conditions. Recording the trajectories of the particles in molecular dynamics simulations, we can identify how particle hopping and cluster merging events are realized. We find that the number of particles involved in these processes is of comparable size and that under-populated clusters (with ∼70% of the average cluster size) are prone for merging processes. Theoretical predictions about the density-dependence of the average cluster size and of the nearest cluster-distance are confirmed within good accuracy. © *2014 AIP Publishing LLC*. [http://dx.doi.org/10.1063/1.4896055]

I. INTRODUCTION

In the past decade, systems consisting of ultrasoft particles have attracted a steadily increasing attention in the field of soft matter physics as they are considered as promising model systems for coarse-grained neutral[1–5] and charged[6–8] macromolecules. Ultrasoft particles exhibit a vastly different behavior than their classical, hard-core counterparts, for instance Lennard-Jones particles, as their mutual interaction is bounded and usually purely repulsive. Under certain conditions (see further below), such ultrasoft particles are able to form stable aggregates (clusters) of overlapping particles.[9] At low densities, these clusters form together with isolated particles a disordered liquid state.[10] However, as the density is increased and/or the temperature is lowered, the system undergoes a first order phase transition into ordered structures – so-called cluster crystals[10–15] – where the lattice positions are populated by clusters of overlapping particles. Although the formation of stable aggregates of mutually repelling particles might seem counter-intuitive at first sight, the general principles of this phenomenon are meanwhile well understood:[12–14] it has been demonstrated in Ref. 16 that this type of clustering occurs due to a Kirkwood instability when the interaction potential between ultrasoft particles assumes negative values in Fourier space.

Monomer-based computer simulations have provided unambiguous evidence that such ultrasoft potentials provide a realistic coarse-grained description of the effective interactions between certain macromolecules, for example, amphiphilic dendrimers.[17] In this case, the dendrimers self-assemble into clusters of overlapping molecules in an effort to minimize the contact between the solvophobic core and the solvent. In simulations based on monomeric-models it was shown (i) that these particles are indeed able to form in the disordered, fluid phase aggregates of overlapping particles[18] and (ii) that the ordered cluster phases formed by these dendrimers are mechanically stable.[19]

So far, the static properties of ultrasoft cluster-forming systems have been studied extensively, providing evidence that they show several unexpected and intriguing features as compared to their hard matter counterparts. In contrast, only little is known about the response of these systems to external fields such as pressure or mechanical shear.[20] The present contribution is dedicated to a detailed, simulation-based study on how cluster crystals react on an externally applied pressure. Our investigations are motivated by the fact that previous studies on the equilibrium properties have provided evidence that cluster crystals exhibit a highly unusual response to compression, due to the inherent softness of the constituent particles: increasing the density in cluster crystals does not induce a decrease in the lattice constant (as one would intuitively expect), but instead leads to a linear increase in the average occupation number per lattice site.[10,12,13] The redistribution of particles is realized via two key processes, namely, *particle hopping* and *cluster merging*. Particle hopping is a characteristic transport mechanism in cluster forming systems,[21–23] where particle jumps extending over multiple lattice site are commonplace (both in- and out-of-equilibrium). In contrast, merging of clusters essentially never occurs under equilibrium conditions due to the high energy barriers that separate adjacent clusters in the crystal. Under these conditions merging of two clusters would be an energetically highly unfavorable process. This novel response to compression is unique for ultrasoft clustering systems, setting them apart from conventional hard matter crystals, which

[a)]Electronic mail: marta.montes.saralegui@tuwien.ac.at
[b)]Electronic mail: arashn@princeton.edu

can react to pressure only through the shrinking of the lattice constant.

In an effort to understand the interplay between hopping and merging events we have investigated a system of ultrasoft, cluster-forming particles; their interaction will be specified in Sec. II. For computational reasons and in an effort to enhance the transparency of the processes we have restricted ourselves to a two-dimensional nanodrop where the clusters form a regular, hexagonal lattice. The motivation to study a finite system instead of a bulk crystal lies on our initial hypothesis that the merging events will occur close to the surface in contact with the pressure bath. In an effort to study these effects we have realized *NPT* conditions by bringing the system into contact with an external combined pressure- and temperature-bath, formed by ideal gas particles.[24,25] The pressure (P_t) and temperature (T_t) of the barostat and thermostat are controlled via the number of ideal gas particles and their velocities, respectively. Pressure and temperature are transferred from this reservoir to the nanocrystal through a repulsive cross-interaction. The trajectories of all particles involved are calculated in standard molecular dynamics simulations. The pressure is increased repeatedly in steps of ΔP at fixed T_t, thereby temporarily inducing non-equilibrium conditions under which both hopping and merging processes can occur. In these time-windows the particle trajectories are recorded for the subsequent analysis: by identifying hopping and merging events along compression experiments (carried out for different target temperatures and pressure increments) we are able to shed more light into their complex interplay.

The remainder of this manuscript is organized as follows: in Sec. II we present the model system, and provide a brief summary of our simulation scheme. A detailed discussion of the results is then given in Sec. III. The manuscript is concluded with a summary and an outlook. A description of the data analysis scheme can be found in the Appendix.

II. MODEL AND SIMULATION METHOD

We consider a two-dimensional system of N ultrasoft particles, which interact via the GEM4 potential,

$$\Phi(r) = \epsilon \exp[-(r/\sigma)^4]. \tag{1}$$

In this expression, σ and ϵ are length- and energy-parameters, respectively, which will be used henceforward as respective units. In addition, we used the following reduced, dimensionless quantities: the number-density $\rho^* = \rho\sigma^2$, temperature $T^* = k_B T/\epsilon$ (k_B being the Boltzmann constant), pressure $P^* = P\epsilon/(k_B\sigma^2)$, and time $t^* = \sigma\sqrt{m/\epsilon}$ (m being the mass of the particles). In what follows, we will drop the asterisks for the sake of simplicity. For most of our investigations (and if not otherwise stated) we have considered ensembles of $N = 6144$ particles. We have tested our simulations for finite-size effects by conducting additional runs at selected state points for $N = 20\,736$ and $N = 2816$, and were not able to observe any impact on our results.

NPT-conditions are achieved by coupling the GEM4 particles to a combined pressure- and heat-bath, which is explicitly modeled by N_g ideal gas particles. These particles do not exhibit any self-interaction (hence "ideal"), but interact only with the GEM4 particles via an inverse power potential,

$$\Psi(r) = \left(\frac{\sigma_b}{r}\right)^{12}. \tag{2}$$

We set the parameter σ_b to σ, guaranteeing thereby that the ideal gas particles do not penetrate into the region occupied by the GEM4 particles. A cut-off radius of $R_c = 2\sigma_b$ has been introduced; beyond this cut-off radius this cross-interaction vanishes. Since the equation of state of the ideal gas particles is known exactly, we can accurately control the pressure and temperature of the enclosed cluster-forming system by varying the number of gas particles, N_g, and their velocities (see Refs. 24 and 25 for a more detailed discussion).

Similar as in preceding applications of this technique,[24] we have replaced the original, complex-shaped minimum volume for the ideal gas particles (given by those particle positions that lie within R_c of each GEM4 particle) by a more generous volume, built up by quadratic cells of length 2σ due to computational considerations. Outside this volume, ideal gas particles are not represented explicitly anymore, but the infinite extension of the pressure- and heat-bath is modeled by a flow of particles through the boundary surface: the number of particles entering the system and the distribution of their velocities are properly derived from the equation of state.[24] Figure 1 shows a typical snapshot of the total system (ultrasoft particles and ideal gas particle reservoir), where GEM4 particles have already formed an ordered cluster phase.

The trajectories of both particle species have been evaluated by standard molecular dynamics simulations, using a velocity-Verlet integration scheme with a time-increment of $\delta t = 0.002t$. Configurations were saved every 1000 time steps, i.e., every $2t$. Compression of the system is achieved by repeatedly increasing the imposed pressure by an increment, ΔP. After each step, we let the system relax to reach the desired target temperature T_t. We consider the system in

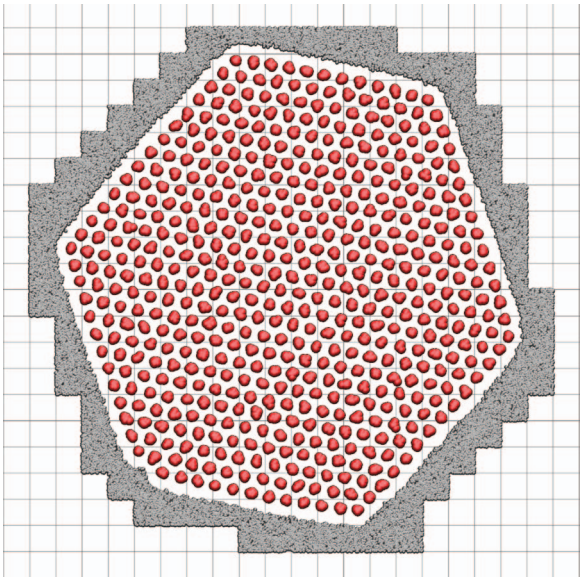

FIG. 1. Simulation snapshot of a system consisting of 6144 GEM4 particles (red) which is in contact with a combined barostat and thermostat comprised of ideal gas particles (grey). The square lattice in the outer region defines the underlying cell structure of the ideal gas reservoir (see text).

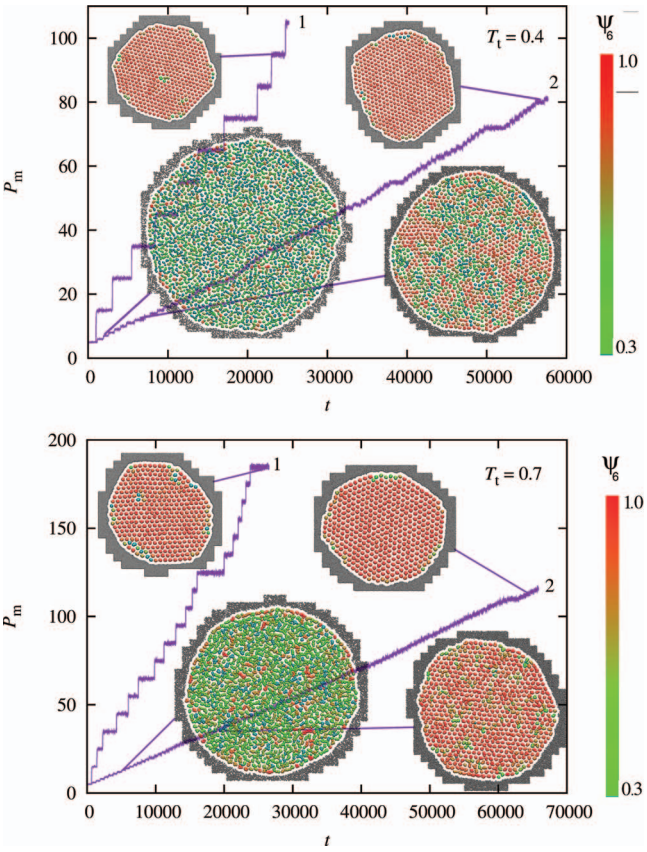

FIG. 2. Pressure *vs.* time during typical compression processes, where pressure increments of $\Delta P = 10$ (curve labelled as 1) and $\Delta P = 1$ (curve labelled as 2) have been applied. The corresponding target temperatures are indicated in the upper right corners of the panels. In addition, typical snapshots of the GEM4 particles are shown for selected pressure values: grey dots represent particles from the combined pressure- and temperature bath; GEM4 particles are color coded according to the value of the order parameter Ψ_6 defined in Eq. (3).[27]

equilibrium when the temperature measured in the GEM4 population, T_m, lies within an interval $[T_t - \Delta T, T_t + \Delta T]$, with $\Delta T/T_t = 1\%$. Then the system is simulated at equilibrium over a time window $t_w = 500\,t$, i.e., 250 000 simulation steps, during which the system properties are recorded. This procedure is then repeated until the desired pressure range has been covered. Typical snapshots along compression processes are shown in Figure 2, where we typically required $N_g \sim 33\,000$ for $P = 40$ and $N_g \sim 85\,000$ for $P = 130$ for a system containing $N = 6144$ GEM4 particles (in both cases $T_t = 0.3$).

III. RESULTS

We have performed compression experiments for the systems specified in Sec. II at representative target temperatures, namely, for $T_t = 0.3$, 0.4, 0.5, 0.6, and 0.7. Here, we applied different pressure increments, i.e. $\Delta P = 1$, 5, 10, and 25, to analyze the effect of compression strength. In the following we focus on results obtained for the target temperatures $T_t = 0.4$ and $T_t = 0.7$ and for the pressure increments $\Delta P = 1$ and $\Delta P = 10$, since these state points are representative for the entire parameter regime studied here. For certain quantities we also include results obtained for the remaining temperatures and pressure increments and we will then discuss temperature trends in our data.

The four panels of Figure 3 show the measured temperature in the GEM4 system T_m as a function of time for all combinations of T_t and ΔP. In addition, these graphs show the number of particles involved in hopping (N_h) and in merging (N_m) events as functions of time. The grey vertical lines delimit time intervals during which – according to the compression protocol specified in Sec. II – the pressure is kept constant. In each panel the left-most black vertical line indicates the time at which we declare (via visual inspection) that the system has reached the ordered cluster phase; from this point onwards we start with the cluster analysis. The purple arrows delimit those time windows that we have studied in more detail (see discussion below).

From Figure 2 and a first qualitative inspection of the panels of Figure 3 we can make the following general observations of the compression experiment:

(i) Each time the pressure has been increased by ΔP we see an immediate jump in temperature (ΔT_m), followed by pronounced fluctuations in T_m. For a moderate pressure increment $\Delta P = 1$ the variations in T_m are considerably less pronounced than for $\Delta P = 10$. In the former case, these fluctuations level off rather fast and consequently it takes the system considerably less time to reach its target temperature and thus its equilibrium state. The length of the time intervals during which the pressure is kept constant (t_P) is therefore shorter for moderate pressure increments. However, the length of the time intervals is not inversely proportional to ΔP; thus for $\Delta P = 10$ we are able to obtain a final value for the pressure that is by a factor 2.6 ($T_t = 0.4$) to 3.2 ($T_t = 0.7$) higher than for $\Delta P = 1$ in a simulation of comparable runtime.[26]

(ii) The values of t_P are substantially smaller at a higher target temperature, where the temperature fluctuations are considerably larger: as a consequence, the system reaches its equilibrium state considerably faster and simulations of comparable length lead at $T_t = 0.7$ to pressure values that are by a factor 1.4 ($\Delta P = 1$) to 1.75 ($\Delta P = 10$) higher than those achieved at $T_t = 0.4$.

(iii) For a given ΔP-value, the time-intervals during which the pressure is kept fixed differ in their length. Additional and independent compression runs under the same conditions provide evidence that the lengths of the time-intervals for a specific pressure value can differ. In Figure 4 we summarize this information by plotting $\langle t_P \rangle$ against the target temperature T_t for all investigated pressure increments ΔP. Here it is clearly visible that $\langle t_P \rangle$ decreases as a function of T_t and increases as a function of ΔP for a fixed T_t-value. The errorbars provide an impression about the spread in the t_P-values. Nevertheless, these differences in the equilibration protocol do not affect the relevant data that we have extracted from these runs.

We now investigate the impact of the temperature and the pressure increment on the number of particles involved in hopping (N_h) and merging (N_m) events. Temperature has a strong influence on these two processes: while at high

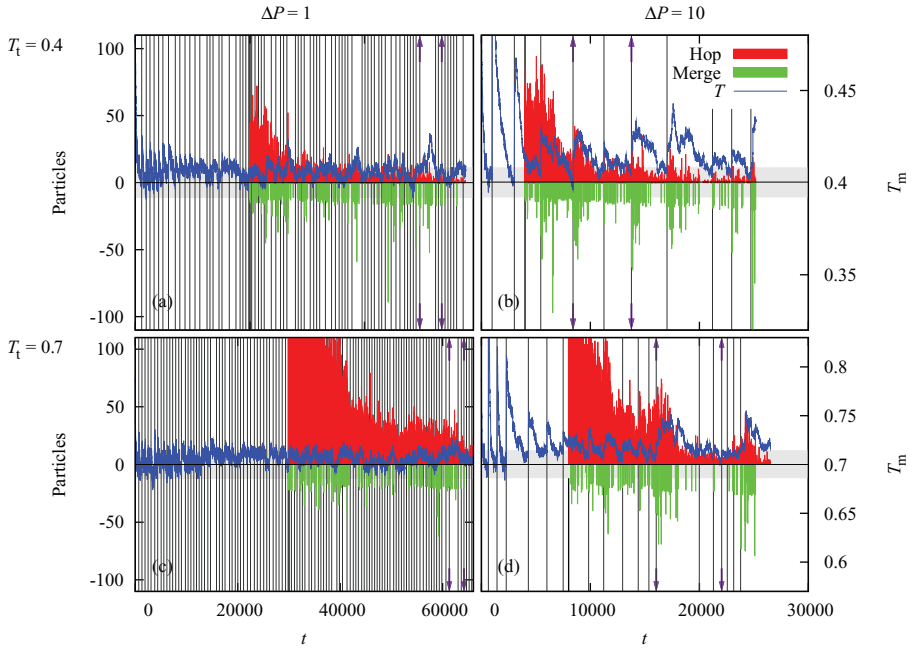

FIG. 3. Instantaneous temperature T_m (blue line) as well as the number of particles involved in hopping N_h (red vertical bars) and merging events N_m (green vertical bars) *vs.* time. Panels (a) and (b) show results for target temperature $T_t = 0.4$, while panels (c) and (d) show results for $T_t = 0.7$. Panels (a) and (c) correspond to $\Delta P = 1$, while panels (b) and (d) show results for $\Delta P = 10$. N_h and N_m are plotted only over a time range where the ordered, hexagonal cluster crystal has formed. The vertical black line in each panel marks the onset of this regime. The purple arrows delimit the time windows analyzed in detail in Figures 6–9. The grey horizontal bar represents the tolerance interval of temperature, which is ±2% of T_t. Thin grey vertical lines delimit time-intervals during which the pressure is kept constant.

temperatures hopping strongly dominates over merging, we observe at low T_t that N_h and N_m are of comparable size. At this point one should mention that N_h is the result of normal activated hopping processes that constantly take place at finite temperature[22,23] plus hopping events that occur as a response of the system due to the compression. In contrast, merging events essentially only occur as the system is compressed.

As we start our data analysis (i.e., from the vertical black lines onwards shown in Figure 3), there is an initial phase where hopping processes dominate over merging events ($N_h > N_m$); this intermediate time-regime corresponds to a low-order phase. Then, as the system attains a higher order configuration, N_h stabilizes around a constant value comparable to N_m. At this point we can conclude that both hopping and merging are relevant mechanisms responsible for particles rearrangements. For a moderate pressure increment the variations in N_h and N_m are considerably less pronounced than for the case $\Delta P = 10$, where N_h and N_m increase immediately after the pressure increment has been applied: large pressure steps activate the hopping and merging activity.

In what follows, we will provide a more detailed study of the complex interplay between hopping and merging processes of a cluster forming system. In Figure 5 we plotted the normalized size distribution of those clusters that are involved at a given instant in merging processes for different temperatures. We found that – essentially irrespective of temperature – this distribution has its maximum at $n_{occ}/\langle n_{occ}\rangle$

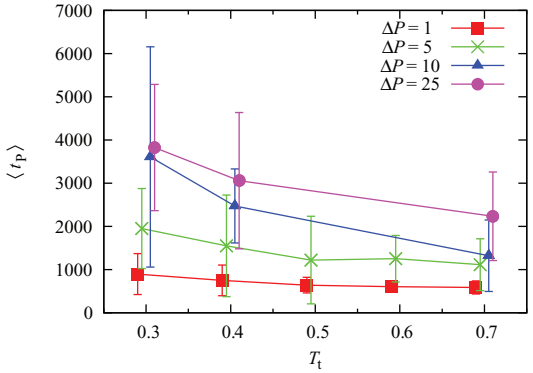

FIG. 4. Average timespan for which the pressure is kept constant $\langle t_P\rangle$ *vs.* target temperature, T_t for various pressure increments ΔP (as labelled). The points have been slightly displaced along the T_t-axis for the sake of clarity. Error bars indicate the spread in the $\langle t_P\rangle$-values.

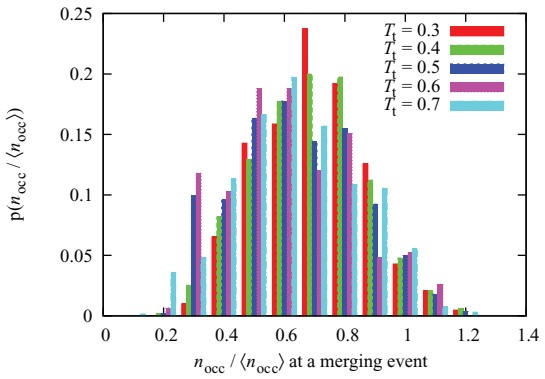

FIG. 5. Probability distribution of the size of the clusters involved in a merging event normalized by the instantaneous global average cluster occupation. Results are shown for simulations at different target temperatures T_t.

~ 0.7, i.e., clusters that are involved in merging processes are smaller in size as compared to the other clusters in the system. We can thus make the following conclusions: ultrasoft, cluster forming systems initially respond to compression through an activated hopping process, which leads to a spatially heterogeneous cluster size distribution. Our original hypothesis that the frequency of merging events will be higher close to the surface could not be confirmed. Since under-occupied clusters feel a strong repulsion from larger, neighboring clusters, they are forced to approach each other and eventually merge. Figure 5 provides evidence that in our system merging events cannot occur without preceding hopping events, the latter ones being responsible for the necessary spatially heterogeneous cluster occupation: if the cluster-size distribution is too narrow (as it occurs in equilibrium) the larger clusters will not be able to exert a sufficiently strong repulsion on the smaller ones to make them merge.

In an effort to provide a more detailed insight of how the properties of the system change during a compression step we have selected for each combination of T_t and ΔP representative compression levels, during which the pressure was kept fixed. These regions are delimited in Figure 3 by the purple arrows, and the characteristic system properties are plotted as functions of time in Figures 6–9. These graphs contain also data from the final part of the preceding pressure interval, offering thus the possibility to trace how the characteristic properties of the system change as we increase the pressure by ΔP.

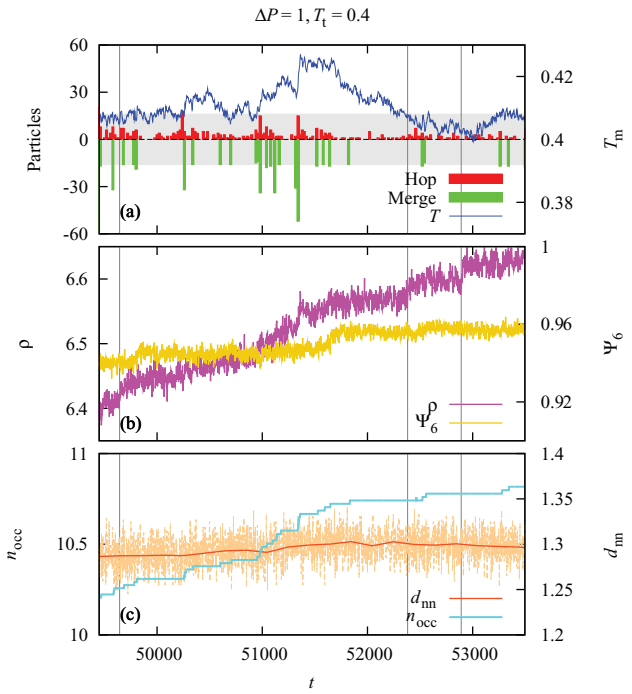

FIG. 6. Variation of typical system properties as functions of time at fixed pressure $P_t = 72$–74 and target temperature $T_t = 0.4$, with $\Delta P = 1$. (a) Number of particles involved in hopping and merging events (N_h and N_m; left y-axis) and target temperature (right y-axis). The grey horizontal bar represents the tolerance interval in temperature, i.e., $\pm 2\%$ of T_t. (b) Number density ρ (left y-axis) and order parameter Ψ_6 (right y-axis). (c) Average occupation number $\langle n_{occ} \rangle$ (left y-axis) and nearest neighbor distance d_{nn} (right y-axis). The dark-orange curve represents a running average over 100 configurations (light-orange) corresponding to 10^5 time steps. The grey vertical line indicates where the pressure step is applied.

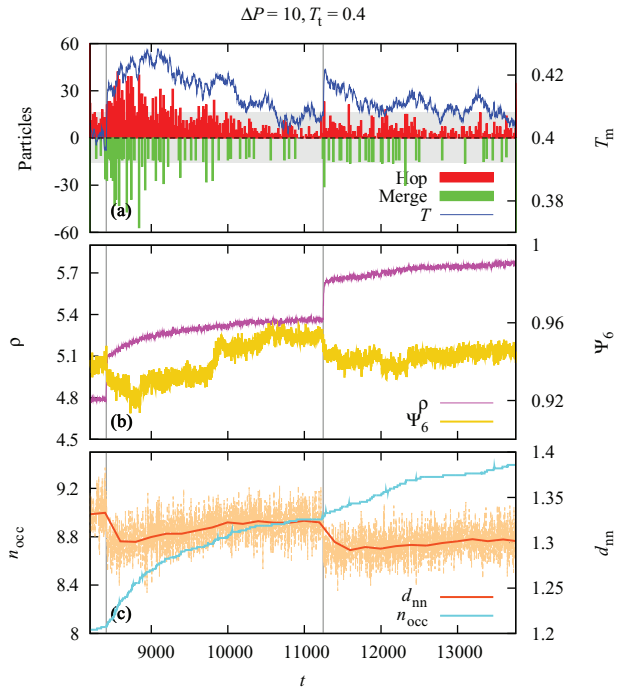

FIG. 7. Same as Figure 6, but for $\Delta P = 10$ at $P_t = 45$–55.

Data compiled in panel (a) of these figures confirm our previously made conclusions: under compression, hopping processes dominate over merging events at high temperature, while at low temperature N_h and N_m attain comparable values; further, the pressure increment has a distinct influence on the absolute numbers of particles involved in these events: the larger ΔP, the higher N_h and N_m. In addition, sudden and substantial changes in the temperature correlate

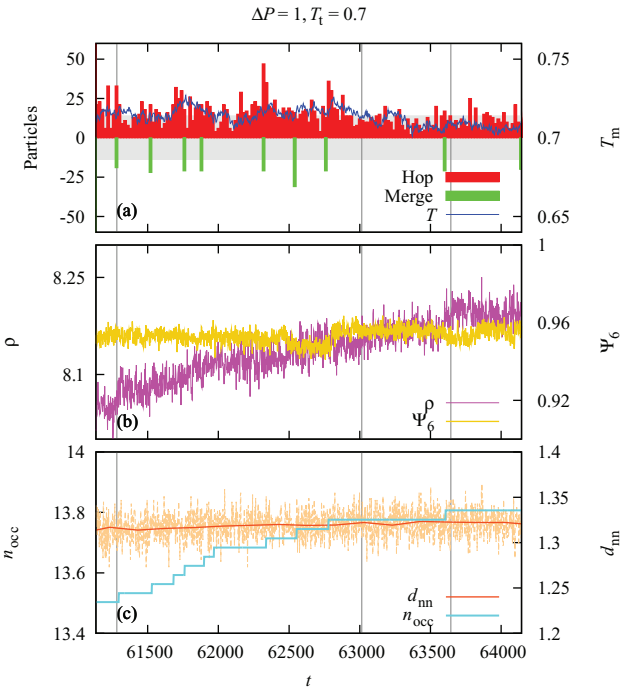

FIG. 8. Same as Figure 6, but for $T_t = 0.7$ and $\Delta P = 1$ at $P_t = 110$–112.

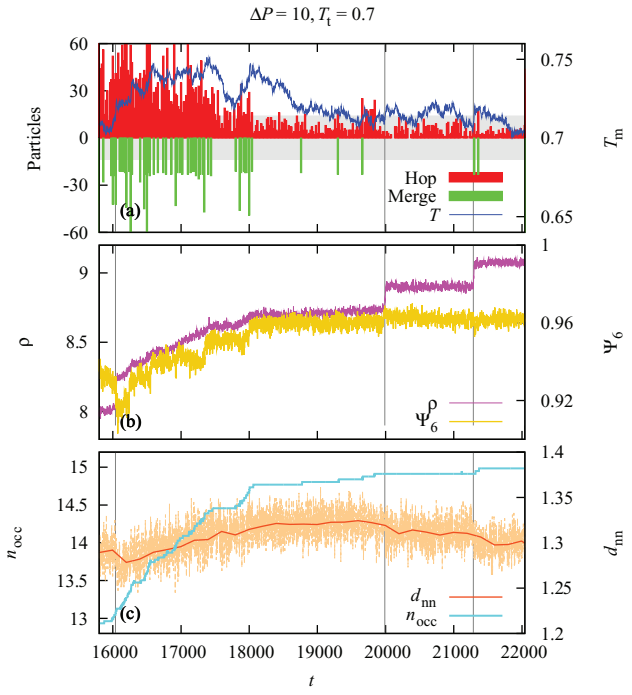

FIG. 9. Same as Figure 6, but for $T_t = 0.7$ and $\Delta P = 10$ at $P_t = 125$–145.

throughout with increased hopping and merging activities in the system.

In panels (b) of Figures 6–9 we plotted the number density ρ and order parameter Ψ_6, which quantifies the hexagonal order in the system. Following Ref. 27, we used

$$\Psi_6 = \frac{1}{N}\sum_j^N \frac{1}{n_j}\sum_k^{n_j} \exp(i6\Theta_{jk}), \tag{3}$$

where n_j denotes the number of nearest neighbors of particle j, and Θ_{jk} the angle between the selected particle and its nearest neighbors. By definition, Ψ_6 attains a value of 1 for a perfectly hexagonal arrangement, while we found $\Psi_6 \approx 0.4$ for the disordered liquid state. For $\Delta P = 1$, the density shows a rather smooth, monotonic increase with time and saturates at its equilibrium value, well before the target temperature has been reached. In contrast, for $\Delta P = 10$ we observe a sudden increase of ρ when the pressure increment is applied; however, after this initial and abrupt jump we observe the same behavior of the density as for $\Delta P = 1$. This behavior was found independent of temperature T_t.

In panel (c) we quantified the two mechanisms through which a cluster crystal of ultrasoft particles can react to a reduction in volume: (i) either by shrinking the lattice spacing or (ii) via the deletion of some lattice positions. We can measure the former by d_{nn}, the position of the highest peak of the radial distribution function, and the latter through the average cluster occupation, $\langle n_{occ}\rangle$. For $\Delta P = 1$ we find that d_{nn} is essentially constant over the time-window, irrespective of the temperature. In contrast, for $\Delta P = 10$ we observe a sudden drop in the lattice spacing when the pressure increment is applied, followed by a very slow increase until d_{nn} eventually saturates. The average occupation number, $\langle n_{occ}\rangle$, increases monotonically irrespective of the value of ΔP, until it saturates where the system is back in equilibrium, i.e., the target temperature has been reached (within the given interval of tolerance). Combining these data, we can draw the following conclusions: the discontinuous increase in density induced by a pressure increase is related to a shrinkage of the lattice spacing while the subsequent monotonic increase in density is realized by a steady deletion of lattice positions, reflected by the increase of $\langle n_{occ}\rangle$. Hence, only large ΔP values can provoke a sudden shrinkage of the lattice constant.

In Figure 10 we show d_{nn} and $\langle n_{occ}\rangle$ of our cluster forming system along the entire compression experiments for the two T_t- and the two ΔP-values considered. In these panels the black vertical line indicates the time at which we declare (via visual inspection) that the system has reached the ordered cluster phase. We observe that d_{nn} assumes in the initial fluid phase values of $d_{nn} \simeq 0.5$. As compression proceeds, an additional peak at $r \simeq 1.4$ appears. There is a transition region, where the value of d_{nn} jumps back and forth between these two values (0.5 and 1.4). As the density increases, the peak at $r \simeq 1.4$ prevails and finally, one indicator that the system forms an ordered phase is the disappearance of the first peak at $r \simeq 0.5$.

From the data shown in Figure 10 we observe as a general trend in all compression experiments that d_{nn} exhibits an initial monotonic decay with time. Eventually this quantity levels off to a value of $d_{nn} \simeq 1.28$, independent of the target temperature and the pressure increment. At this point it is appropriate to recall theoretical predictions for cluster forming systems of ultrasoft particles, based on density functional theory (DFT):[13] using a mean-field (MF) picture, DFT predicts a density-*independent* lattice constant, i.e., a feature that is equivalent to a linear increase of the average cluster occupancy, $\langle n_{occ}\rangle$, with density. Further, for the ordered cluster phase of a two dimensional GEM4 system $d_{nn} \simeq 1.42$ is predicted.

From an analysis of our simulation data we can make the following conclusions: (i) $\langle n_{occ}\rangle$ shows indeed a linear dependence on the density ρ (see the insets of Figure 10 which display the equilibrium values of d_{nn} as functions of the density ρ). (ii) The moderate decrease of d_{nn} with density can be attributed to the compression protocol which leads (even for moderate pressure increments) to lattice defects in the ordered cluster phase. This becomes apparent from the color-coded snapshots in Figure 2: the number of "green" clusters provides a qualitative measure of how far a configuration deviates from an ideal, six-fold coordinated cluster crystal. Indeed, current investigations, which will be published in an upcoming contribution, provide evidence that these defects can be removed by an annealing process: keeping the pressure constant, the system is first heated up until it has completely melted and is then cooled down to the desired target temperature. As we track the density of the resulting annealed ordered cluster phases for different pressure values we find that the resulting lattice constant d_{nn} is indeed density-*independent* and attains a value of $d_{nn} \simeq 1.37$. The reason for these discrepancies in the lattice constant obtained via compression (with and without annealing) and via the theoretically predicted value is definitely not due to finite size effects: additional simulations for $N = 2816$ and $N = 20736$ GEM4-particles lead to the same value for

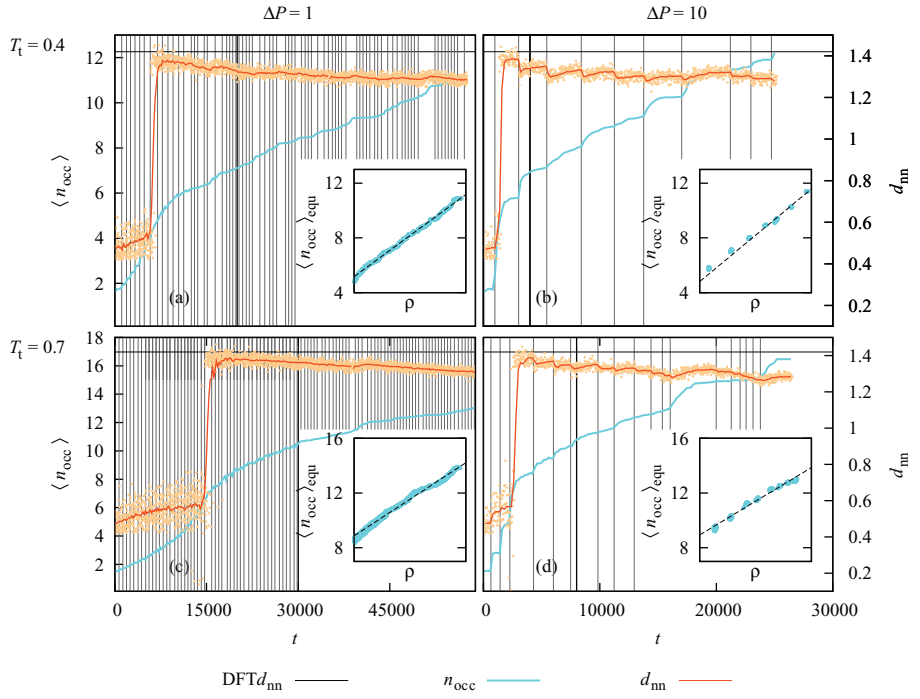

FIG. 10. Main panels: nearest neighbor distance, d_{nn} (from simulations and DFT calculations), and average cluster occupancy, $\langle n_{occ} \rangle$, as functions of time. The dark-orange curve represents a running average over 100 configuration (light-orange) corresponding to 10^5 time steps. $T_t = 0.7$ in panels (a) and (b), while $T_t = 0.4$ in panels (c) and (d). $\Delta P = 1$ in panels (a) and (c), and $\Delta P = 10$ in panels (b) and (d). Thin grey vertical lines mark the onset of the regime where the ordered hexagonal cluster crystal has formed. Insets: average cluster occupation at equilibrium (i.e., when the temperature deviates within a tolerance of ±2% from the target temperature) as a function of density. The dotted line represents a linear fit of $\langle n_{occ} \rangle_{equ}$.

d_{nn}. We therefore conclude that these discrepancies are most likely due to the simplifying assumptions within the DFT/MF approach.

IV. CONCLUSIONS

We have investigated a two-dimensional nanodrop composed of ultrasoft, cluster forming particles that is exposed to a combined thermo- and barostat, realized via ideal gas particles. We controlled the target pressure and temperature of the system through the number and velocity of these particles, respectively. We found that the system formed a hexagonal arrangement of clusters of overlapping particles (a so-called cluster crystal) when the pressure exceeded a certain threshold value. By repeatedly increasing the pressure of the system in small increments we imposed non-equilibrium conditions over a certain time-period, until it eventually recovers its equilibrium.

We found that the dynamics of the systems are dominated by hopping and merging processes. While particle hopping (i.e., migration of individual particles from one cluster site to a neighboring one) can be studied in equilibrium computer simulations, merging of clusters (i.e., the unification of two adjacent, underpopulated particle aggregates) can only be induced under some external driving force, such as an external pressure or an external shearing force. By considering different target temperatures and different values for the pressure increment we were able to shed light onto the microscopic details of how a cluster crystal reacts to external pressure. During most of the compression experiment a comparable number of particles are involved in hopping and merging processes, providing evidence of the importance of the two mechanisms for rearranging particles. Analyzing the properties of the clusters that are involved in merging processes we find that – irrespective of the target temperature – clusters that are by ∼70% underpopulated are prone for cluster merging. Recording the cluster size, n_{occ}, and the cluster distance, d_{nn}, during the compression process we can confirm that the respective equilibrium values of these quantities fulfill (within a good accuracy) the theoretically predicted behavior: n_{occ} increases linearly with density, while d_{nn} remains essentially constant over the entire pressure range, differing, however, by a few percent from the predicted theoretical value.

ACKNOWLEDGMENTS

We thank Michael Grünwald and Christoph Dellago (both at University of Vienna) for useful discussions. This work has been supported by the Marie Curie ITN-COMPLOIDS (Grant Agreement No. 234810), by the Austrian Science Fund (FWF) under Project Nos. P23910-N16 and F41 (SFB ViCoM), and by the WK "Computational Materials Science" of the Vienna University of Technology. A.N. acknowledges financial support by the Princeton Center for Complex Materials (PCCM), a U.S. National Science Foundation Materials Research Science and Engineering Center (Grant No. DMR-0819860).

APPENDIX: ANALYSIS

The analysis of our data is carried out in a five-step procedure: in **step one** of our cluster analysis of a given particle

configuration we have used the scheme detailed in the Appendix of Ref. 22. As an initial value for the cut-off distance, r_c, which is required for grouping neighboring particles to a cluster, we chose $r_c = 0.42\sigma$. This value corresponds to the position of the first minimum of the radial pair distribution. Then we calculated the individual (n_{occ}) and the average ($\langle n_{occ} \rangle$) occupancy of each cluster as well as its spatial extent, quantified by its radius of gyration, r_g.

The first class of clusters that requires special treatment in **step two** are oversized clusters, i.e., all clusters with an occupation number larger than $N_{occ}^{max} = 1.6\langle n_{occ} \rangle$. Such clusters can appear either because (a) two under-occupied clusters have merged or (b) because a hopping particle is located at this very instant between two clusters and the cluster analysis could not identify them as separate aggregates ("fused clusters"). A suitable quantity for distinguishing these two cases is the radius of gyration r_g, and we set $r_g^{max} = 1.4\sigma$ to identify fused clusters. This test is carried out via the following iterative algorithm: we identify for each particle of such a cluster its average number of neighbors; all particles that have less neighbors than this average value are put aside for the moment and the cluster analysis is repeated with the remaining particles, whereby the original cluster meanwhile might have split up into two (or more) (sub-)clusters. If the radii of gyration of the resulting clusters are still larger than 1.4σ, the value of r_c is reduced by 10% and steps 1 and 2 are repeated until the r_g-values of the emerging clusters are smaller than 1.4σ. The isolated particles that have been previously put aside during the algorithm are then reintegrated and assigned to the respective nearest cluster.

In **step three** we focus on small clusters ($n_{occ} < 3$) which are most probably migrating particles. They are assigned to the respective nearest cluster, but are not included in the evaluation of its center-of-mass.

Finally, we focus in **step four** on clusters that are separated by a distance that is smaller than 0.65σ, which we consider as merged clusters. This particular value for the threshold distance represents a reasonable choice in view of the fact that the lattice constant of our cluster crystal assumes values close to 1.37σ.

Finally we identify and analyze in **step five** merging and cluster separation events. If in a compression step two clusters have merged from one configuration I to the subsequent one ($I + 1$), one of the cluster identities is maintained for the further analysis while the other one is put idle. If, in contrast, in an expansion step, a cluster has separated into two (sub-)clusters from one configuration to the following one, the subcluster that is closer to the original aggregate keeps the identity of the latter, while for the other subcluster a new identity is created. All other aggregates of configuration ($I + 1$) will carry on the cluster identity of those aggregates that are closest in configuration I to their actual position. If the association of a particle to a cluster changes from one configuration to the subsequent one, this particle is identified as a hooping particle; relevant information about the particle and the cluster it belonged to is stored. Through this criterion also particles involved in merging processes are identified as hopping particles; using now the information obtained in the preceding cluster-tracking analysis we can finally separate hopping particles from those that are involved in merging processes in a final step.

Of course, steps two–six are applicable only in the ordered solid phase. The transition from the disordered to the ordered phase is determined prior to the cluster analysis by visual inspection. For the disordered configurations only the first step of the analysis is performed.

[1] J. Dautenhahn and C. K. Hall, Macromolecules **27**, 5399 (1994).
[2] A. A. Louis, P. G. Bolhuis, J. P. Hansen, and E. J. Meijer, Phys. Rev. Lett. **85**, 2522 (2000).
[3] M. Ballauff and C. N. Likos, Angew. Chem. Int. Ed. **43**, 2998 (2004).
[4] S. Prestipino, F. Saija, and P. V. Giaguinta, J. Chem. Phys. **123**, 144110 (2005).
[5] M. Bohn and D. W. Heermann, J. Chem. Phys. **132**, 044904 (2010).
[6] D. Gottwald, C. N. Likos, G. Kahl, and H. Löwen, Phys. Rev. Lett. **92**, 068301 (2004).
[7] A. R. Denton, Phys. Rev. E **67**, 011804 (2003).
[8] P. B. Warren and A. J. Masters, J. Chem. Phys. **138**, 074901 (2013).
[9] W. Klein, H. Gould, R. A. Ramos, I. Clejan, and A. I. Mel'cuk, Physica A **205**, 738 (1994).
[10] B. M. Mladek, D. Gottwald, G. Kahl, M. Neumann, and C. N. Likos, Phys. Rev. Lett. **96**, 045701 (2006).
[11] K. Zhang, P. Charbonneau, and B. M. Mladek, Phys. Rev. Lett. **105**, 245701 (2010).
[12] B. M. Mladek, D. Gottwald, G. Kahl, M. Neumann, and C. N. Likos, J. Phys. Chem. B **111**, 12799 (2007).
[13] C. N. Likos, B. M. Mladek, D. Gottwald, and G. Kahl, J. Chem. Phys. **126**, 224502 (2007).
[14] B. M. Mladek, P. Charbonneau, C. N. Likos, D. Frenkel, and G. Kahl, J. Phys.: Condens. Matter **20**, 494245 (2008).
[15] N. B. Wilding and P. Sollich, Europhys. Lett. **101**, 10004 (2013).
[16] C. N. Likos, A. Lang, M. Watzlawek, and H. Löwen, Phys. Rev. E **63**, 031206 (2001).
[17] B. M. Mladek, G. Kahl, and C. N. Likos, Phys. Rev. Lett. **100**, 028301 (2008).
[18] D. A. Lenz, B. M. Mladek, C. N. Likos, G. Kahl, and R. Blaak, J. Phys. Chem. B **115**, 7218 (2011).
[19] D. A. Lenz, R. Blaak, C. N. Likos, and B. M. Mladek, Phys. Rev. Lett. **109**, 228301 (2012).
[20] A. Nikoubashman, G. Kahl, and C. N. Likos, Phys. Rev. Lett. **107**, 068302 (2011).
[21] A. J. Moreno and C. N. Likos, Phys. Rev. Lett. **99**, 107801 (2007).
[22] D. Coslovich, L. Strauss, and G. Kahl, Soft Matter **7**, 2127 (2011).
[23] M. Montes-Saralegui, A. Nikoubashman, and G. Kahl, J. Phys.: Condens. Matter **25**, 195101 (2013).
[24] M. Grünwald and C. Dellago, Mol. Phys. **104**, 3709 (2006).
[25] M. Grünwald, C. Dellago, and P. L. Geissler, J. Chem. Phys. **127**, 154718 (2007).
[26] Typical simulation runs for $\Delta P = 1$ ($\Delta P = 10$) extend over six (three) days on a supercomputer using 12 parallel cores.
[27] K. J. Strandburg, Rev. Mod. Phys. **60**, 161 (1988).